Supporting Information

Expansion of oil palm and other cash crops causes an increase of land surface temperature in Indonesia

Clifton R. Sabajo[1,2†], Guerric le Maire[3], Tania June[4], Ana Meijide[1], Olivier Roupsard[3,5], Alexander Knohl[1,6]

[1] University of Goettingen, Bioclimatology, 37077 Göttingen, Germany

[2] AgroParisTech – Centre de Montpellier, Agropolis International, 648 rue Jean-François Breton, 34093 Montpellier, France

[3] CIRAD, UMR Eco&Sols, F-34398 Montpellier, France

[4] Agrometeorology Laboratory Department of Geophysics and Meteorology, Faculty of Mathematics and Natural Sciences, Bogor Agricultural University (IPB), Indonesia

[5] CATIE (Centro Agronómico Tropical de Investigación y Enseñanza / Tropical Agriculture Centre for Research and Higher Education), 7170 Turrialba, Costa Rica

[6] University of Goettingen, Centre of Biodiversity and Sustainable Land Use (CBL), 37073 Goettingen, Germany

[†] Correspondence: Clifton R. Sabajo, University of Goettingen, Bioclimatology, Büsgenweg 2, 37077 Göttingen, Germany. E-mail: csabajo@uni-goettingen.de

Telephone: +49 (0) 551 39 12114

Supporting information to this article is arranged as follows:

S3. ET from satellite images with SEBAL

Fig. S3.1 Analysis of the steps involved in deriving the input for deriving ET from Landsat images with SEBAL

Fig. S3.2 Comparison of ET derived from upper anchor and lower anchor pixels.

Table S3.1. u*, rah, LE and H measured at a young and mature oil palm plantation

S4. Mean LST, NDVI, Albedo and NDVI extracted for 7 land cover types

Fig. S4.1 Mean LST, NDVI, Albedo and NDVI extracted from Landsat LST images for 7 land cover types

S5. Difference in LST, NDVI, albedo and ET between Forest (FO) and 6 other land cover types

Fig. S5.1 Differences in LST (ΔLST), NDVI (ΔNDVI), Albedo (ΔAlbedo) and Evapotranspiration (ΔET) between other land covers (RU, MOP, PF, YOP, UB and CLC) and forest (FO) in the Jambi province

S6. Statistical analysis

Table S6.1 ANOVA statistics

Table S6.2 Post-hoc Tukey HSD test statistics

Table S6.3 The relation LST-Albedo-NDVI-ET separated by land cover type

S7. Comparison of MODIS LST to in situ measured canopy LST

Fig. S7.1 MODIS LST compared to in situ measured canopy surface temperature.

S8. Comparison of MODIS Air temperature with locally measured air temperature

Fig. **S8.1** MODIS Air temperature compared with in situ measured air temperatures

S9. Land use change analysis for the Jambi province for 2000 – 2010

Table S9.1 Land use change (1990) – 2000 – 2010

Table S9.2 Contribution of land cover change to total LST increase

S1. Surface temperature retrieval from Landsat thermal images

Surface temperature from Landsat ETM+ is derived in a series in steps using the red (R), near-infrared (NIR) and thermal infrared (TIR) band, and follows the method described by Bastiaanssen et al. (1998a, 1998b) and summarized in table S1.

Table S1.1. Steps in the retrieval of the surface temperature from Landsat 7 TIR band

Computation step	**Symbol**	**Unit**	**Formulation**
1. Conversion of the digital number (DN) of the VIS and TIR bands to spectral radiance	L_λ	$W/m^2/sr/\mu m$	$L_\lambda = \frac{LMAX - LMIN}{QCALMAX - QCALMIN} \times (DN - QCALMIN) + LMIN$
2. Conversion of spectral radiance bands to reflectance[#] (λ = 1, 2, 3, 4, 5, 7)	ρ_λ	-	$\rho_\lambda = \frac{\pi \cdot L_\lambda}{ESUN_\lambda \cdot cos\theta \cdot d_r}$
3. Normalized Difference Vegetation Index	NDVI	-	$NDVI = \frac{\rho 4 - \rho 3}{\rho 4 + \rho 3}$
4. Soil Adjusted Vegetation Index	SAVI	-	$SAVI = \frac{(1 + L)(\rho 4 - \rho 3)}{(L + \rho 4 + \rho 3)}$
5. Transformed SAVI to pseudo-LAI[§]	SAVI"	-	$SAVI'' = \frac{-\ln\left(\frac{0.69 - SAVI}{0.59}\right)}{0.91}$
6. Narrowband emissivity	εNB	-	$\varepsilon NB = 0.97 + 0.0033\ SAVI''$; $SAVI'' < 3$ (a) $\varepsilon NB = 0.98$; $SAVI'' \geq 3$ (b)
7. Broadband emissivity	ε0	-	$\varepsilon 0 = 0.95 + 0.01\ SAVI''$; $SAVI'' < 3$ (a) $\varepsilon 0 = 0.98$; $SAVI'' \geq 3$ (b)
8. Atmospheric correction of the thermal radiance band	Rc	$W/m^2/sr/\mu m$	$Rc = \frac{L6 - Rp}{\tau NB} - (1 - \varepsilon NB)Rsky$
9. Surface temperature calculation	LST	K	$LST = \frac{k2}{\ln\left(\frac{\varepsilon NB \cdot k1}{Rc} + 1\right)}$

Where:

DN	the digital number of each pixel of band λ	$W/m^2/sr/\mu m$
LMAX	calibration constant specific for each Landsat sensor (see table S1.2)	$W/m^2/sr/\mu m$
LMIN		
QCALMAX	highest and lowest range values for rescaled radiance in DN (see table S1.2)	$W/m^2/sr/\mu m$
QCALMIN		
$ESUN_\lambda$	the mean solar exo-atmospheric irradiance for each band (see table S1.3)	$W/m^2/\mu m$
θ (θ = 90º- β)	solar incidence angle	angular degrees
β	sun elevation from meta data satellite image	angular degrees
d_r	the relative distance between earth and sun $d_r = 1 + 0.033 \cos (DOY \frac{2\pi}{365})$	-
DOY	the sequential time of the year The unit of the angle ($DOY \times \frac{2\pi}{365}$) is in radians.	-
ρ_4	surface reflectance of band 4 (NIR, 750 – 900 nm)	-
ρ_3	surface reflectance of band 3 (VIS Red, 630 – 690 nm)	-
L	adjustment factor to minimize the backscatter effect of soil background reflectance through the canopy (0.1)	-
τNB	band average atmospheric transmittance	-
Rp	effective bandpass upwelling radiance (or Path radiance)	$W/m^2/sr/\mu m$
Rsky	effective bandpass downwelling radiance	$W/m^2/sr/\mu m$
k1 (= 666.09)	sensor constants for converting band 6 to surface temperature	$mW/cm^2/sr/\mu m$
k2 (= 1282.71)		K

#: when using Landsat surface reflectance product, this step is not necessary. §The transformed SAVI is considered here to be equal to the LAI.

References: 4: Huete (1988); 5: Bulcock and Jewitt (2010); 6, 7: Bastiaanssen et al. (1998a, 1998b); 8: Wukelic et al. (1989); Coll et al. (2010).

Table S1.2. LMIN and LMAX values for Landsat 7 ETM+ (Landsat 7 Science User Data Handbook Chap. 11, 2002) in units $W\ m^{-2}\ sr^{-1}\ \mu m^{-1}$ (after July 1, 2000)

	Band number	**1**	**2**	**3**	**4**	**5**	**6**	**7**	**8**
Low gain	LMAX	293,7	300,9	234,4	241,1	47,57	17,04	16,54	243,1
	LMIN	-6,2	-6,4	-5	-5,1	-1	0	-0,35	-4,7
High gain	LMAX	191,6	196,5	152,9	157,4	31,06	12,65	10,8	158,3
	LMIN	-6,2	-6,4	-5	-5,1	-1	3,2	-0,35	-4,7
	QCALMAX	255	255	255	255	255	255	255	255
	QCALMIN	1	1	1	1	1	1	1	1

Table S1.3. Mean solar exo-atmospheric irradiance (ESUNλ) for Landsat 7 ETM+ (Landsat 7 Science User Data Handbook, Chapter 11, 2002). Units are in $W/m^2/\mu m$.

	Band 1	Band 2	Band 3	Band 4	Band 5	Band 61	Band 62	Band 7
Landsat 7	1969	1840	1551	1044	225.7	1	1	82.07

S2. Atmospheric correction of the thermal band

For the atmospheric correction of the thermal radiance, the correction parameters τ, Rp and Rsky are derived from NASA's online atmospheric correction calculator (Barsi et al., 2003, 2005) which requires the following input: latitude and longitude, elevation, air temperature, surface pressure and relative air humidity. This Web-based ACT has been developed for TM and ETM+ thermal data (Barsi et al., 2005; Coll et al., 2010). It uses atmospheric profiles from the National Centers for Environmental Prediction (NCEP) interpolated to a particular location, date and time, and the MODTRAN-4 code to calculate the atmospheric-correction parameters for the bandpass of either the TM or ETM+ thermal band for a given date and site (Coll et al., 2010). The output of the online atmospheric parameter calculator is: band average atmospheric transmission (τ), effective bandpass upwelling radiance (Rp) and the effective bandpass downwelling radiance (Rsky). The calculated atmospheric parameters can be applied to a given scene to retrieve the surface temperature for the area of interest. The thermal band (L6) is corrected for atmospheric effects after Wukelic et al. (1989) and Coll et al. (2010) as:

$$\mathrm{Rc} = \frac{\mathrm{L6} - \mathrm{Rp}}{\tau} - (1 - \varepsilon\mathrm{NB})\mathrm{Rsky}$$

The input data required for the atmospheric calculator and the output parameters required for atmospheric correction and applied to the selected Landsat satellite image are summarized in table S2.1.

Table S2.1. Input and output parameters for/from NASA´s online atmospheric correction parameter calculator applied to two satellite images of the study area. Results in this study were based on the satellite image acquired on 2013-06-19.

Location	**Date (yyyy-mm-dd):**	**2013-06-19**
Input	Lat	-1.966
	Lon	102.601
	GMT Time:	3:13
Input surface conditions	Surface altitude (km):	0.046
	Surface pressure (mb):	1002.90
	Surface air temperature (C):	28.35
	Surface relative humidity (%):	50.90
Output summary	Band average atmospheric transmission:	0.67
	Effective bandpass upwelling radiance:	2.68
	Effective bandpass downwelling radiance:	4.25

Band average atmospheric transmission = τ, effective bandpass upwelling radiance = Rp ($W/m^2/sr/\mu m$), effective bandpass downwelling radiance = Rsky ($W/m^2/sr/\mu m$).

S3. ET from satellite images using SEBAL

Steps in deriving ET with the SEBAL

1. Net radiation (Rn, W/m^2) is calculated as:

$$Rn = (1 - \alpha)\, S_d\downarrow + \varepsilon_a \sigma T_a^4 - (1 - \varepsilon_0)\, \varepsilon_a \sigma T_a^4 - \varepsilon_0 \sigma LST^4 \quad \text{(Eq. S1)}$$

Rn is the net radiation (W/m^2);

$S_d\downarrow$ is the incoming shortwave solar radiation (in W/m^2) at the surface;

α is the surface albedo (-)

ε_0: the surface emissivity (-), derived from the NDVI and is described in table S1.

ε_a: the atmospheric emissivity (-), estimated with:

$$\varepsilon a = 1 - 0.26 \cdot \exp\{-7.77 \times 10^{-4}) \cdot (273.15\text{-}Ta)^2\} \quad \text{(Eq. S2)}$$

σ: Stephan-Boltzmann constant (5.67 × 10^{-8} W/m^2/K^4);

LST: the surface temperature (K) derived from Landsat;

T_a: is the near surface air temperature (K).

2. Soil heat flux (G, W/m^2) is calculated as:

$$G = Rn \cdot \frac{LST - 2\ \ .15}{\alpha} \cdot (0.0038\alpha + 0.0074\alpha^2) \cdot (1 - 0.98NDVI^4) \quad \text{(Eq. S3)}$$

G is the ground heat flux (W/m^2);

Rn is the net radiation (W/m^2);

LST: the surface temperature (K) derived from Landsat;

α is the surface albedo (-)

3. Sensible heat flux (H, W/m^2) is calculated in a series of steps as:

a. z_{0m} (the particular momentum roughness length for each pixel) is derived from an empirical relation between z_{0m} and NDVI and albedo as

$$z_{0m} = e^{\left(a \cdot \frac{NDVI}{\alpha}\right) + b} \quad \text{(Eq. S4)}$$

coefficients *a* and *b* are derived from the linear relation between:

$$\ln z_{0m} \sim a \cdot \frac{NDVI}{\alpha} + b \quad \text{(Eq. S5)}$$

From figure S3.1b we derived *a* and *b* as:
a = 0.24
b = -2.29

b. friction velocity (u*, m/s) at weather station (u_{200}, m/s) is derived as:

$$u^* = \frac{k \cdot u_z}{ln\left(\frac{z}{z_{0m}}\right)} \quad \text{(Eq. S6)}$$

c. the wind speed 200 m above the weather station (u_{200}, m/s) is derived as:

$$u_{200} = u^* \frac{ln\left(\frac{200}{z_{0m}}\right)}{k} \quad \text{(Eq. S7)}$$

k = von Karman's constant = 0.41

z_{0m} = as calculated with Eq. S4

c. The aerodynamic resistance to heat transport r_{ah} (s/m) is calculated as:

$$r_{ah} = \frac{ln\left(\frac{z_2}{z_1}\right)}{u^* \cdot k} \quad \text{(Eq. S8)}$$

d. the near surface temperature difference (dT) for each pixel is defined as:

$$dT = b + a\ LST \quad \text{(Eq. S9)}$$

a and *b* are correlation coefficients which are derived by:
i. selecting hot and cold pixels (a.k.a. anchor pixels) in the LST image
ii. using an excel sheet the coefficients *a* and *b* are derived from several iterations

e. finally sensible heat (H) is estimated as:

$$H = \rho \cdot Cp \frac{a\ LST + b}{r_{ah}} \quad \text{(Eq. S10)}$$

r_{ah} = aerodynamic resistance to heat transport r_{ah} (s/m)
ρ = 1.16 kg/m^3 (air density)
Cp = 1004 J/kg/K (air specific heat)

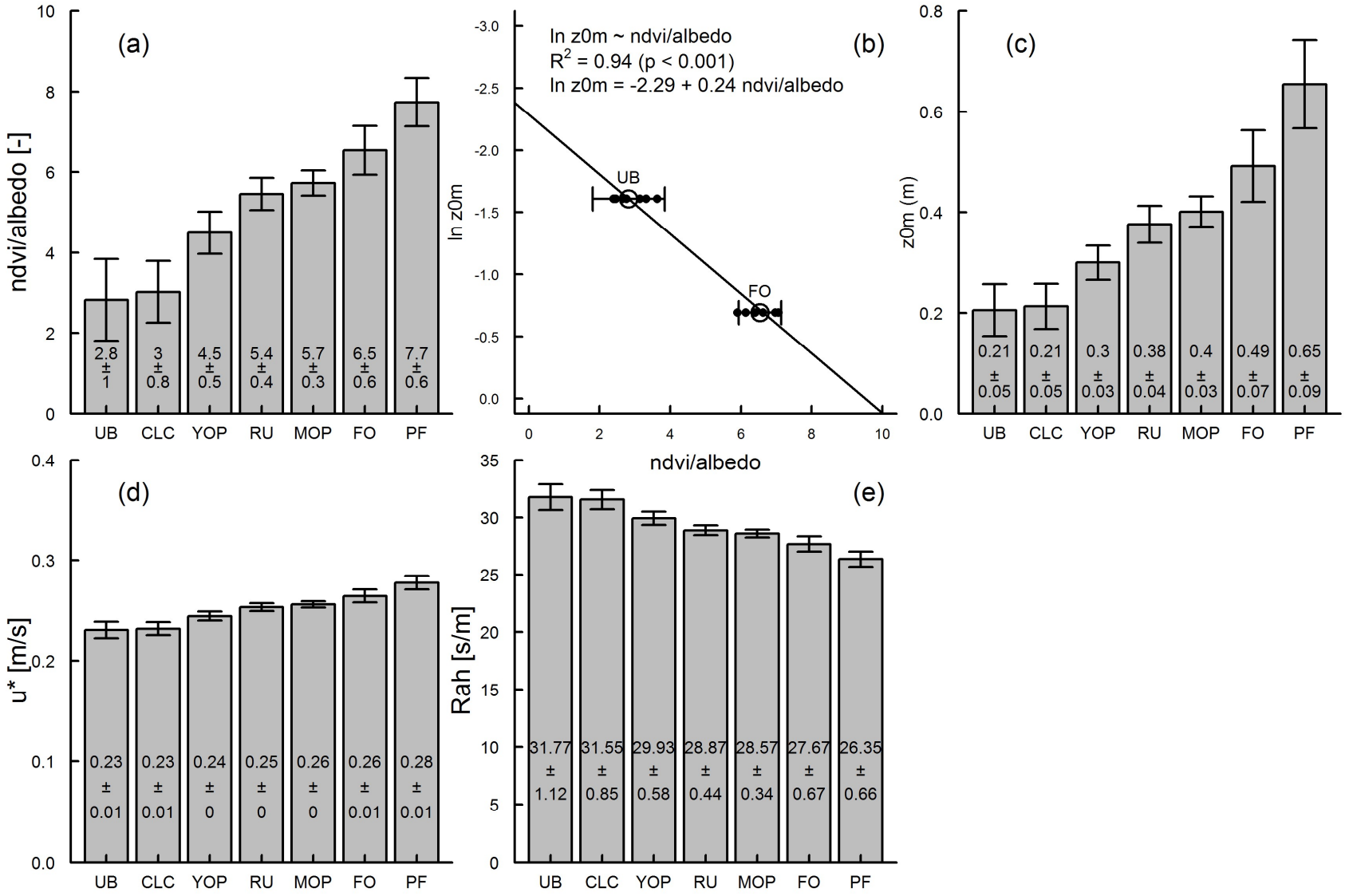

Fig. S3.1 Analysis of the steps involved in deriving the input for deriving ET from Landsat images with SEBAL.

We calculated $u*$ and r_{ah} for a young and mature oil palm plantation (table S3.1). These were calculated from meteorological measurement on these locations. Because the satellite image was acquired outside the time period in which meteorological measurements were made, we selected dates and times that had similar conditions on the day the image was acquired. We used incoming shortwave radiation as a main criteria (> 690 Wm^{-2} and < 720 Wm^{-2}, between 10.00 and 11:00 am local time). $u*$ and r_{ah} derived from the satellite image show a certain level of agreement with the $u*$ and r_{ah} calculated from meteorological data.

4. Latent heat flux (LE, W/m^2) is estimated as residual from Net radiation, Ground heat and sensible heat flux as:

$$LE = Rn - G - H \quad \text{(Eq. S11)}$$

5. Instantaneous evapotranspiration (ET, mm/hr) for each pixel is estimated from LE as:

$$ET_{inst} = 3600 \frac{LE}{\lambda} \quad \text{(Eq. S12)}$$

3600 is the time conversion from seconds to hours
λ = latent heat of vaporization (2.43×10^6 J/kg)

We tested different combinations of 5 hot and 5 cold pixels, that could serve as anchor pixels, and then compared the effects of anchor pixel selection on the ET output. Our comparison showed that the anchor pixels we selected showed an overall effect on the magnitude of ET of less than 10% and had no effect on the ranking of the ET by land use type (Fig. S3.2).

We calculated *LE* and *H* for a young and mature oil palm plantation (table S3.1). These were calculated from flux measurements on these locations. Because the satellite image was acquired outside the time period in which meteorological measurements were made, we selected dates and times that had similar conditions on the day the image was acquired. *LE* and *H* derived from the satellite image show some agreement with the *LE* and *H* calculated from meteorological data.

The technical description can be found in Bastiaanssen et al. (1998a, 1998b).

Table S3.1. $u*$, r_{ah}, LE and H measured at a young and mature oil palm plantation

	Young Oil Palm Plantation (YOP)		**Mature oil Palm Plantation (MOP)**	
	Lower limit§	Upper limit§	Lower limit§	Upper limit§
u* **(m/s)**	0.40 ± 0.15	0.47 ± 0.18	0.12 ± 0.02	0.37 ± 0.11
r_{ah} (s/m)	24.14 ± 11.80	26.92 ± 12.17	22.93 ± 5.20	54.97 ± 7.13
LE (W/m^2)	215.77 ± 61.05	226.22 ± 68.29	413.67 ± 109.54	441.00 ± 109.76
H (W/m^2)	138.34 ± 50.85	140.57 ± 51.32	90.11 ± 32.64	97.25 ± 33.56

§ The table shows 2 values for $u*$, r_{ah}, LE and H. These values were calculated for the lower (> 690 W/m^2) and upper (< 720 W/m^2)limit of incoming solar radiation we selected to match conditions on the day the satellite image was acquired.

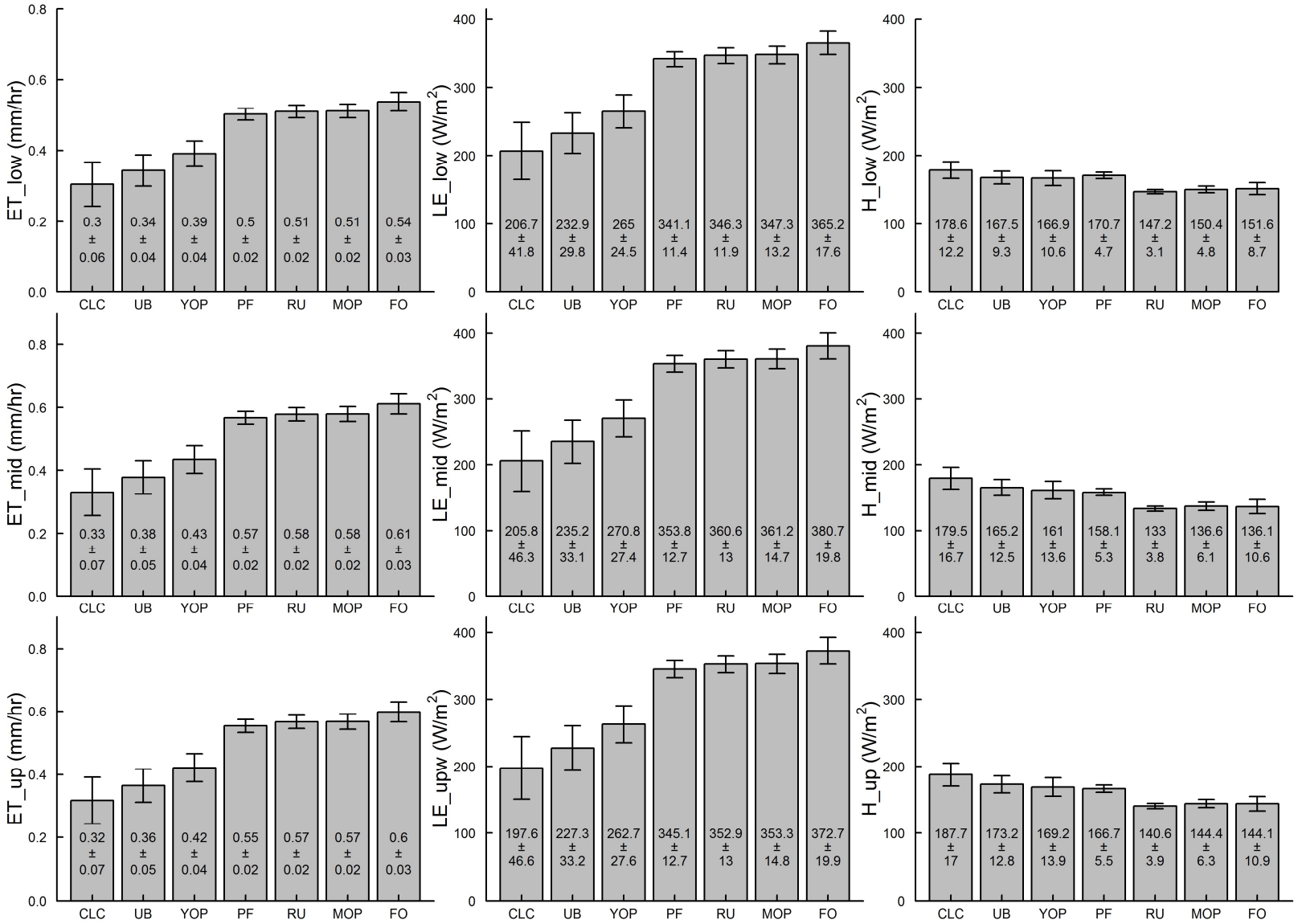

Fig. S3.2 ET, LE and H derived with SEBAL.

S4. Mean LST, NDVI, Albedo and NDVI for 7 land cover types

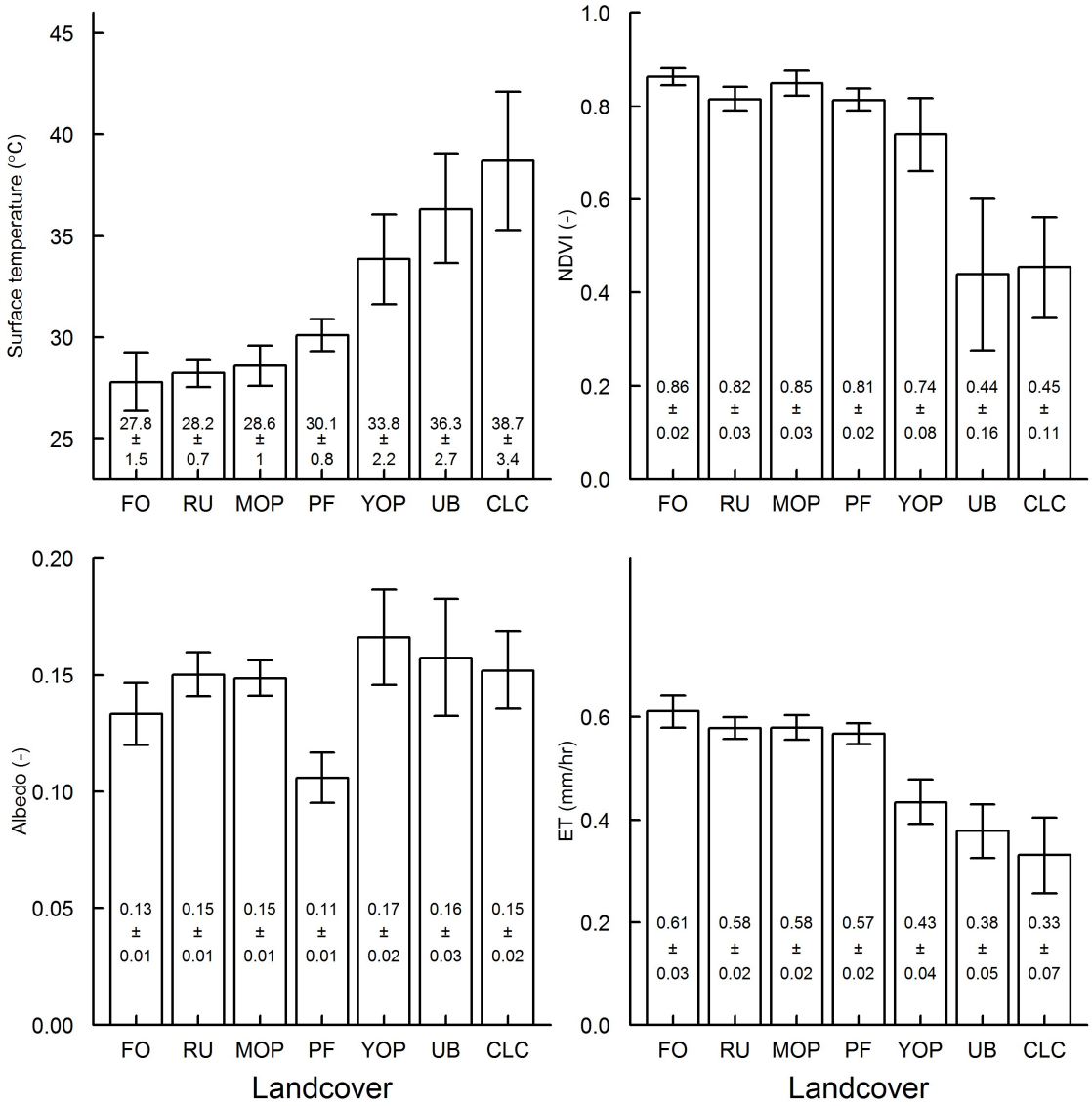

Fig. S4.1 Mean LST, NDVI, Albedo and NDVI extracted from Landsat LST images for 7 land cover types. The values were extracted from small plots that could only be used for Landsat images.

S5. Difference in LST, NDVI, albedo and ET between Forest (FO) and 6 other land cover types

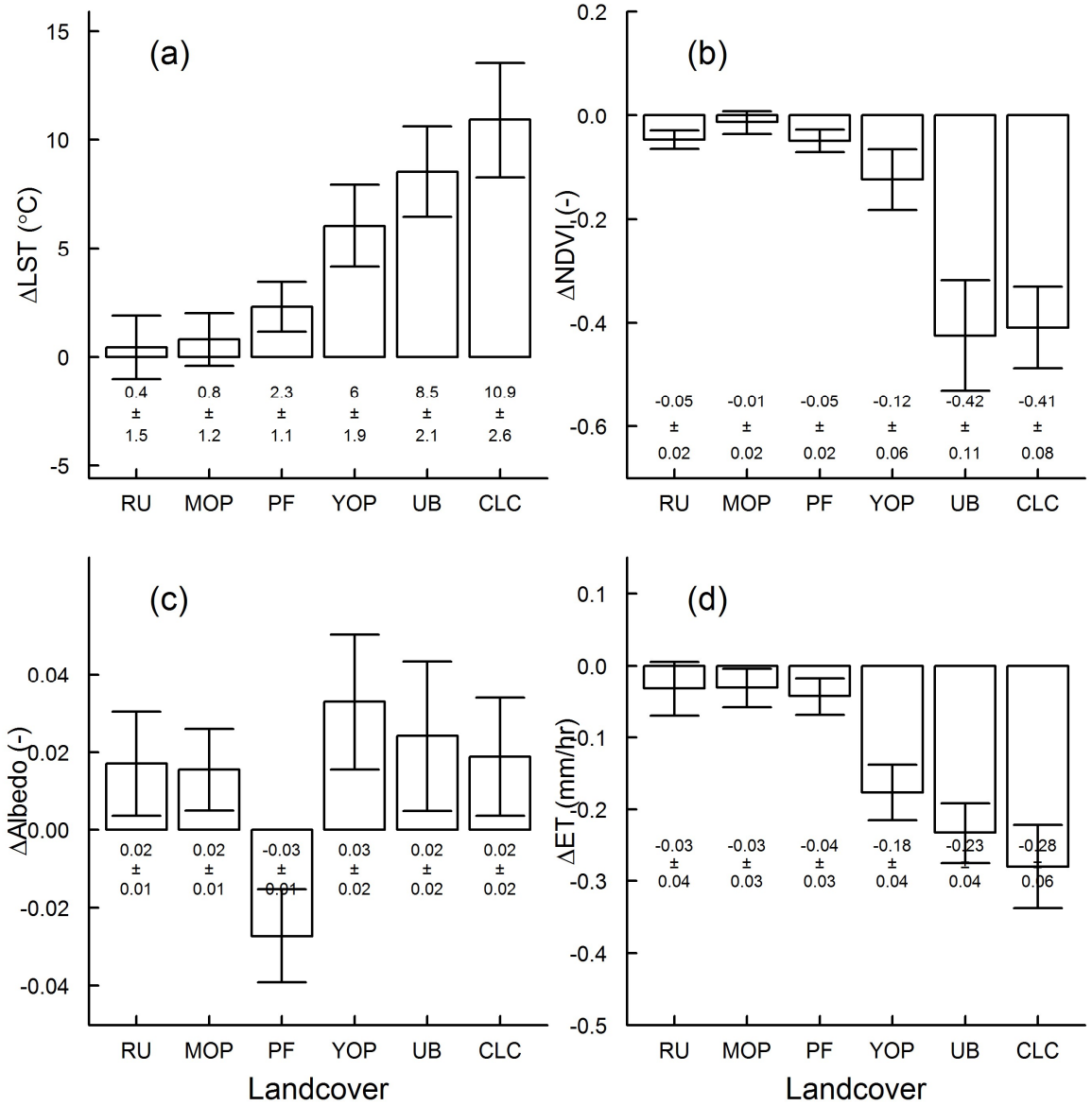

Fig. S5.1 Differences (mean ± SD) in surface temperature (ΔLST), normalized difference vegetation index (ΔNDVI), Albedo (ΔAlbedo) and Evapotranspiration (ΔET) between other land covers (RU, MOP, PF, YOP, UB and CLC) and forest (FO) in the Jambi province, derived from the Landsat LST image acquired on 19 June 2013 at 10:13 am local time.

The standard deviation of 2 means is calculated as the 'pooled standard deviation':

$$sd = \sqrt{\frac{(n1-1)sd1^2 + (n2-1)sd2^2}{n1+n2-2}}$$

n1: sample size population 1 (here: the number of pixels of land cover class Forest, FO)
n2: sample size population 2 (here: the number of pixels of land cover class *i* (*i* = RU, MOP, PF, YOP, CLC, UB)
sd1: standard deviation of the mean of the first population (here: Forest, FO)
sd2: standard deviation of the mean of the second population *i* (*i* = RU, MOP, PF, YOP, CLC, UB)

S6. Statistical analysis

Table S6.1 ANOVA statistics

		Df	Sum Sq.	Mean Sq.	F value	Pr(>F)
L6	Group	6	5033	839	24073	***
	Residuals	41583	1449	0		
Rc	Group	6	13444	2241	25597	***
	Residuals	41583	3640	0		
LST	Group	6	657323	109554	26240	***
	Residuals	41583	173612	4		
Albedo	Group	6	17.0	2.84	11492	***
	Residuals	41583	10.3	0.00		
NDVI	Group	6	1197	200	32402	***
	Residuals	41583	256	0		
ET	Group	6	464	77.3	41141	***
	Residuals	41583	78	0.0		

*** : $p = 2 \times 10^{-16}$

Table S6.2 Post-hoc Tukey HSD test statistics

		Land cover					
L6		**UB**	**FO**	**MOP**	**YOP**	**PF**	**CLC**
	FO	0.00000					
	MOP	0.00000	0.00000				
	YOP	0.00000	0.00000	0.00000			
	PF	0.00000	0.00000	0.00000	0.00000		
	CLC	0.00000	0.00000	0.00000	0.00000	0.00000	
	RU	0.00000	***0.79912***	***0.90144***	0.00000	0.00000	0.00000
Rc		**UB**	**FO**	**MOP**	**YOP**	**PF**	**CLC**
	FO	0.00000					
	MOP	0.00000	0.00000				
	YOP	0.00000	0.00000	0.00000			
	PF	0.00000	0.00000	0.00000	0.00000		
	CLC	0.00000	0.00000	0.00000	0.00000	0.00000	
	RU	0.00000	***0.83540***	***0.91619***	0.00000	0.00000	0.00000
LST		**UB**	**FO**	**MOP**	**YOP**	**PF**	**CLC**
	FO	0.00000					
	MOP	0.00000	0.00000				
	YOP	0.00000	0.00000	0.00000			
	PF	0.00000	0.00000	0.00000	0.00000		
	CLC	0.00000	0.00000	0.00000	0.00000	0.00000	
	RU	0.00000	0.***78391***	0.***89703***	0.00000	0.00000	0.00000
NDVI		**UB**	**FO**	**MOP**	**YOP**	**PF**	**CLC**
	FO	0.00000					
	MOP	0.00000	0.00000				
	YOP	0.00000	0.00000	0.00000			
	PF	0.00000	0.00000	0.00000	0.00000		
	CLC	0.00000	0.00000	0.00000	0.00000	0.00000	
	RU	0.00000	0.00099	0.05903	0.00000	1.***00000***	0.00000
Albedo		**UB**	**FO**	**MOP**	**YOP**	**PF**	**CLC**
	FO	0.00000					
	MOP	0.00000	0.00000				
	YOP	0.00000	0.00000	0.00000			
	PF	0.00000	0.00000	0.00000	0.00000		
	CLC	0.00000	0.00000	0.00000	0.00000	0.00000	
	RU	0.04009	0.00000	***0.99443***	0.00000	0.00000	***0.99009***
ET		**UB**	**FO**	**MOP**	**YOP**	**PF**	**CLC**
	FO	0.00000					
	MOP	0.00000	0.00000				
	YOP	0.00000	0.00000	0.00000			
	PF	0.00000	0.00000	0.00000	0.00000		
	CLC	0.00000	0.00000	0.00000	0.00000	0.00000	
	RU	0.00000	0.00000	***1.00000***	0.00000	***0.62621***	0.00000

Table S6.3 The relation LST-Albedo-NDVI-ET separated by land cover type.

		Rc			LST	
FO	**α**	**NDVI**	**ET**	**α**	**NDVI**	**ET**
ρ	-0.31	-0.48	-0.96	-0.30	-0.48	-0.96
R^2	0.09	0.06	0.96	0.09	0.06	0.97
β	-4.67	1.42	-6.36	-33.86	10.38	-46.43
Stand. β	-0.31	0.13	-1.01	-0.31	0.126	-1.01
Modelfit (R^2)	0.99			0.99		
RU	**α**	**NDVI**	**ET**	**α**	**NDVI**	**ET**
ρ	0.20	-0.48	-0.89	0.20	-0.48	-0.89
R^2	0.12	0.18	1.29	0.12	0.18	1.29
β	-5.59	1.34	-6.50	-40.89	9.74	-47.47
Stand. β	-0.57	0.37	-1.45	-0.57	0.37	-1.45
Modelfit (R^2)	0.99			0.99		
PF	**α**	**NDVI**	**ET**	**α**	**NDVI**	**ET**
ρ	0.26	-0.30	-0.98	0.26	-0.30	-0.98
R^2	0.07	0.06	1.12	0.07	0.06	1.12
β	-2.87	0.87	-6.22	-20.74	6.26	-44.55
Stand. β	-0.28	0.19	-1.15	-0.28	0.19	-1.146
Modelfit (R^2)	0.99			0.99		
MOP	**α**	**NDVI**	**ET**	**α**	**NDVI**	**ET**
ρ	-0.15	-0.41	-0.95	-0.15	-0.41	-0.95
R^2	0.05	0.11	1.07	0.05	0.11	1.07
β	-5.32	1.42	-6.51	-38.50	10.36	-47.26
Stand. β	-0.30	0.27	-1.12	-0.302	0.27	-1.13
Modelfit (R^2)	0.99			0.99		
YOP	**α**	**NDVI**	**ET**	**α**	**NDVI**	**ET**
ρ	-0.71	-0.58	-0.93	-0.72	-0.58	-0.92
R^2	0.25	0.12	0.87	0.26	0.12	0.86
β	-5.55	0.85	-6.79	-39.11	6.06	-47.52
Stand. β	-0.36	0.21	-0.93	-0.36	0.21	-0.94
Modelfit (R^2)	0.99			0.99		
UB	**α**	**NDVI**	**ET**	**α**	**NDVI**	**ET**
ρ	-0.44	-0.72	-0.89	-0.44	-0.72	-0.89
R^2	0.20	0.02	0.77	0.19	0.02	0.78
β	-6.95	-0.08	-6.40	-47.69	-0.51	-44.22
Stand. β	-0.45	-0.03	-0.87	-0.45	-0.03	-0.87
Modelfit (R^2)	0.99			0.99		
CLC	**α**	**NDVI**	**ET**	**α**	**NDVI**	**ET**
ρ	-0.13	-0.68	-0.98	-0.13	-0.68	-0.98
R^2	0.03	0.05	1.02	0.03	0.04	1.01
β	-6.21	0.35	-7.10	-42.87	1.97	-47.66
Stand. β	-0.20	0.07	-1.05	-0.21	0.06	-1.04
Modelfit (R^2)	0.99			0.99		

All metrics were highly significant ($p = 2\times10^{-16}$).

Abbreviations: FO = Forest, RU = Rubber, PF = Acacia Plantation Forest, MOP = Mature Oil Palm, YOP = Young Oil palm, CLC = Clear cut land, UB = Urban Areas

S7. Comparison of MODIS LST to in situ measured canopy LST

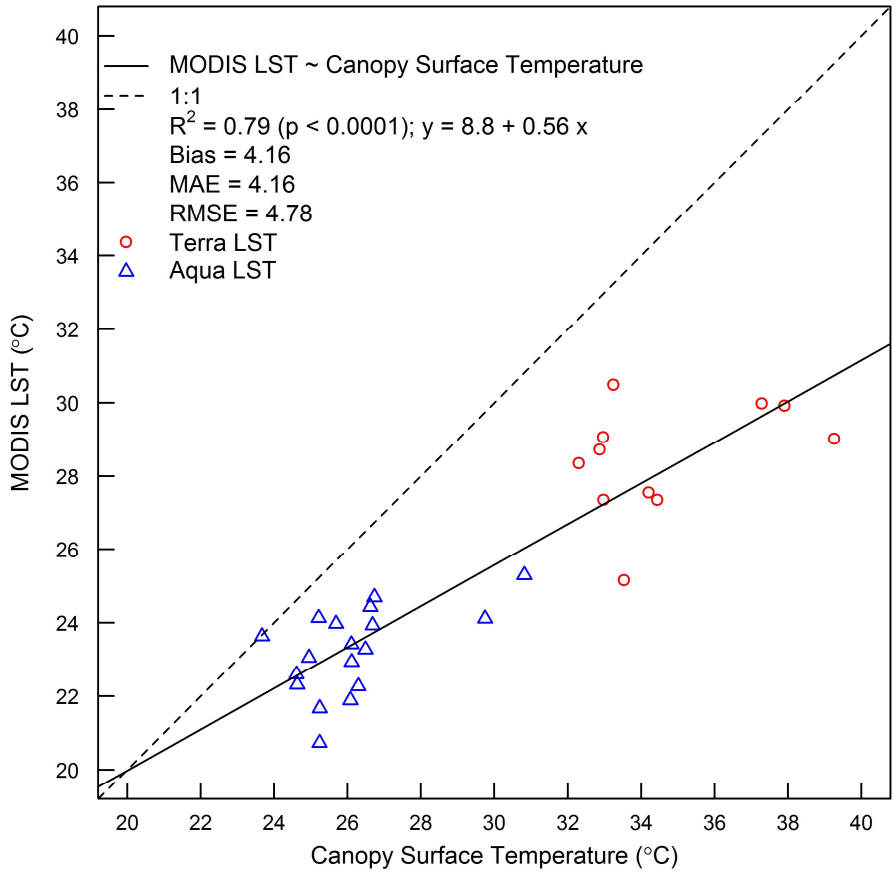

Fig. S7.1 MODIS LST compared to in situ measured canopy surface temperature.
Canopy surface temperature was measured above a homogeneous mature oil palm plantation (12 years old). MODIS LST during 1½ year (mid 2014 – end 2015) was extracted from the pixel covering the location where the *in situ* canopy surface temperature was measured. LST from MODIS on the Terra and Aqua platform were used: Aqua LST in our comparison were measured in the evening hours (around 22:30, local time), Terra LST were measured during morning hours (10:30 am, local time).

Both in situ and MODIS observations are consistent, i.e. the morning temperatures (10:30 am local time vs Terra LST) were warmer than the evening temperatures (10:30 pm local time vs Aqua LST). Differences between the two sources are caused by the comparison of point measurements with pixel values, differences in spatial resolution, differences in soil contribution to the LST estimate, distance in LST measurements and particularly differences in emissivity used for temperature correction. The thermal infrared sensor measuring the surface canopy temperature of the oil palm plantation had fixed default values. MODIS emissivity is derived from 3 thermal bands and adjusted accordingly for every measurement.

S8. Comparison of MODIS Air temperature with locally measured air temperature

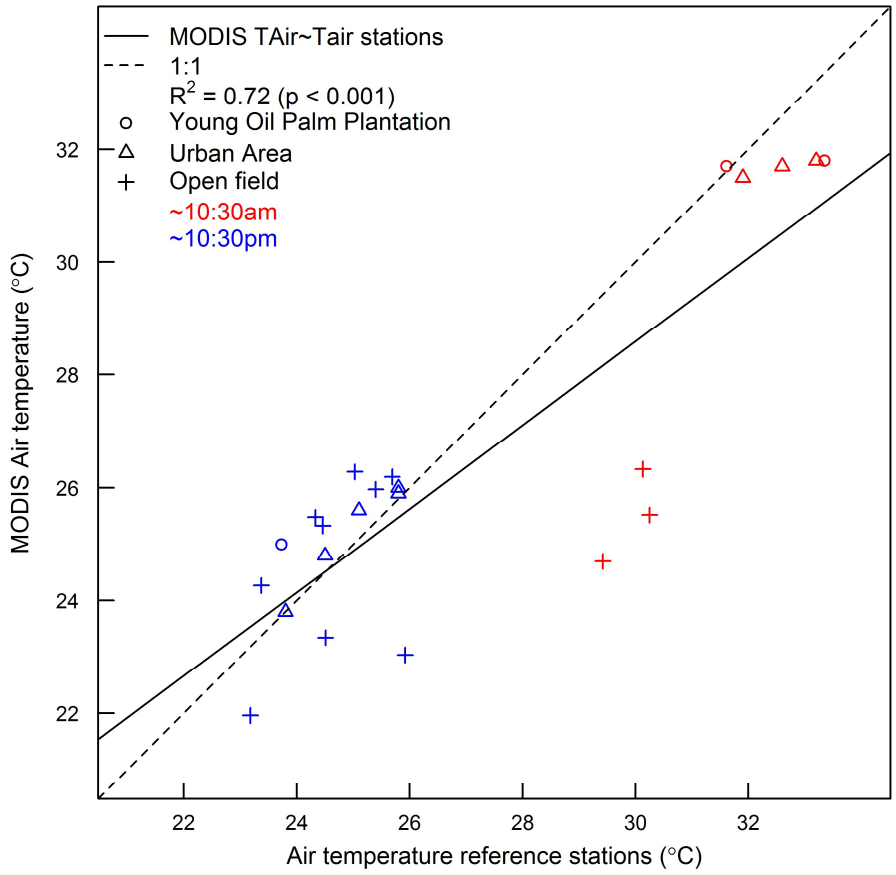

Fig. S8.1 MODIS Air temperature compared with in situ measured air temperatures
Young oil palm plantation (2 years), Urban area and Open field (surrounded by forest) are land use types where the meteorological towers in Jambi were located.
MODIS air temperatures were extracted from the MODIS Air temperature profile product (MOD07) for the three locations.

Both in situ and MODIS observations are consistent, i.e. the morning temperatures (10:30 am, local time) were warmer than the evening temperatures (10:30 pm, local time). Differences between the two sources are caused by the comparison of point measurements with pixel values, differences in spatial resolution and distance in LST measurements.

S9. Land use change analysis for the Jambi province for 2000 - 2010

From Clough et al. (2016) we used the observed LULC for a part of the Jambi province.

Table S9.1 Land use change (1990) – 2000 – 2010

	Area (km^2)			Cover (%)			Change (%)
LULC	**1990**	**2000**	**2011**	**1990**	**2000**	**2011**	**2011-2000**
other	57.83	34.34	52.41	3.3	2.0	3.0	1.03
bush	84.94	263.86	346.99	4.8	15.1	19.7	4.72
OP	204.22	426.51	504.22	11.6	24.3	28.7	4.40
RU	525.90	666.87	668.67	30.0	38.0	38.1	0.06
FO	881.93	361.45	182.53	50.3	20.6	10.4	-10.22
Total	1754.82	1753.03	1754.82	100	100	100	

Table S9.2 Contribution of land cover change to total LST increase

	Increase 2000 – 2010$^{*)}$	**ΔLST**$^{**)}$ **(°C)**	**Contribution to LST (°C)**	**Remark**
RU	0.001	0.4	0.00	1)
MOP	0.022	0.8	0.02	2)
PF	0.000	2.3	0.00	3)
YOP	0.022	6.0	0.13	4)
UB	0.005	8.5	0.04	5)
CLC	0.029	10.9	0.31	6)
Total	0.079		0.51	
Total observed change	0.102			
Missing	0.024			7)

Remarks/explanation:
*) units in fraction of the land cover, which is calculated as the observed change (%, table S9.1) divided by 100
**) warming effect from Fig. 4a (main text)
1) From the observed changes, but seems to be very underestimated, we assume the remaining rubber is mixed with forests as Jungle Rubber
2) MOP = we assume half of the plantations to be mature
3) Not included because increase in area is not known
4) YOP = we assume half of the plantations to be young
5) We assume half of "other" to be urban areas (this assumption is already an overestimation)
6) We assume 50% of the bush to be degraded areas and barren and 50% of the class other to be clear cut land
7) 50% of class "bush" is not included, because this class was not part of our study

References

Barsi, J. A., Barker, J. L. and Schott, J. R.: An Atmospheric Correction Parameter Calculator for a Single Thermal Band Earth-Sensing Instrument, Geosci. Remote Sens. Symp. 2003 IGARSS 03 Proc. 2003 IEEE Int., 5, 3014–3016 vol.5, doi:10.1109/IGARSS.2003.1294665, 2003.

Barsi, J. A., Schott, J. R., Palluconi, F. D. and Hook, S. J.: Validation of a web-based atmospheric correction tool for single thermal band instruments, in Proc. SPIE, Earth Observing Systems X, vol. 5882, San Diego, California, USA., 2005.

Bastiaanssen, W. G. M., Menenti, M., Feddes, R. A. and Holtslag, A. A. M.: A remote sensing surface energy balance algorithm for land (SEBAL) - 1. Formulation, J. Hydrol., 212(1–4), 198–212, doi:10.1016/s0022-1694(98)00253-4, 1998a.

Bastiaanssen, W. G. M., Pelgrum, H., Wang, J., Ma, Y., Moreno, J. F., Roerink, G. J. and van der Wal, T.: A remote sensing surface energy balance algorithm for land (SEBAL).: Part 2: Validation, J. Hydrol., 212–213, 213–229, doi:10.1016/S0022-1694(98)00254-6, 1998b.

Bulcock, H. H. and Jewitt, G. P. W.: Spatial mapping of leaf area index using hyperspectral remote sensing for hydrological applications with a particular focus on canopy interception, Hydrol. Earth Syst. Sci., 14(2), 383–392, doi:10.5194/hess-14-383-2010, 2010.

Clough, Y., Krishna, V. V., Corre, M. D., Darras, K., Denmead, L. H., Meijide, A., Moser, S., Musshoff, O., Steinebach, S., Veldkamp, E., Allen, K., Barnes, A. D., Breidenbach, N., Brose, U., Buchori, D., Daniel, R., Finkeldey, R., Harahap, I., Hertel, D., Holtkamp, A. M., Hörandl, E., Irawan, B., Jaya, I. N. S., Jochum, M., Klarner, B., Knohl, A., Kotowska, M. M., Krashevska, V., Kreft, H., Kurniawan, S., Leuschner, C., Maraun, M., Melati, D. N., Opfermann, N., Pérez-Cruzado, C., Prabowo, W. E., Rembold, K., Rizali, A., Rubiana, R., Schneider, D., Tjitrosoedirdjo, S. S., Tjoa, A., Tscharntke, T. and Scheu, S.: Land-use choices follow profitability at the expense of ecological functions in Indonesian smallholder landscapes, Nat. Commun., 7, 13137, 2016.

Coll, C., Galve, J. M., Sanchez, J. M. and Caselles, V.: Validation of Landsat-7/ETM+ Thermal-Band Calibration and Atmospheric Correction With Ground-Based Measurements, Geosci. Remote Sens. IEEE Trans. On, 48(1), 547–555, doi:10.1109/TGRS.2009.2024934, 2010.

Huete, A. .: A soil-adjusted vegetation index (SAVI), Remote Sens. Environ., 25(3), 295–309, doi:10.1016/0034-4257(88)90106-X, 1988.

Wukelic, G. E., Gibbons, D. E., Martucci, L. M. and Foote, H. P.: Radiometric calibration of Landsat Thematic Mapper thermal band, Remote Sens. Environ., 28(0), 339–347, doi:10.1016/0034-4257(89)90125-9, 1989.